metals

MDPI

Article

A Novel Approach of Microstructure Refinement of TiAl in Laser Beam Welding

Jie Liu [1,2], Shun Guo [1,*], Peng Zhang [2], Tao Ma [2], Zhuo Wang [2], Tongli Wu [3], Li Wang [4] and Kehong Wang [1]

[1] School of Materials Science and Engineering, Nanjing University of Science and Technology, Nanjing 210094, China
[2] Inner Mongolia First Machinery Group Co., Ltd., Baotou 014030, China
[3] School of Mechanical Engineering, Nanjing University of Science and Technology, Nanjing 210094, China
[4] State Key Laboratory of Powder Metallurgy, Central South University, Changsha 410083, China
* Correspondence: guos09@njust.edu.cn

Abstract: Grain refinement through borides is known to be suppressed when TiAl is welded with a laser beam. As β grains do not primarily nucleate on boride at a high cooling rate, a mixture of nitrogen and argon is applied as a protecting gas for the formation of TiN during solidification. The phase transformation is changed correspondingly from Liquid → Liquid + β → β → α + β → α + γ+ β → α_2 + γ + B2 to Liquid → TiN + Liquid → β+ TiN → α + γ + TiN → α_2 + γ+ TiN. It is found that β grains prefer to nucleate heterogeneously on the suspending TiN in the melt with orientation relationship $\{111\}_{TiN}//\{110\}_{\beta}$, leading to refined β grains. α_2 colonies that were thus modified into fine non-dendritic grains. The effects of nitrogen as a shielding atmosphere on the microstructure evolution of TiAl are elaborately studied.

Keywords: TiAl alloy; laser beam welding; microstructure; nitrogen atmosphere; grain refinement

Citation: Liu, J.; Guo, S.; Zhang, P.; Ma, T.; Wang, Z.; Wu, T.; Wang, L.; Wang, K. A Novel Approach of Microstructure Refinement of TiAl in Laser Beam Welding. *Metals* **2023**, *13*, 7. https://doi.org/10.3390/met13010007

Academic Editor: Ruslan R. Balokhonov

Received: 9 November 2022
Revised: 13 December 2022
Accepted: 18 December 2022
Published: 20 December 2022

1. Introduction

TiAl alloys are considered to be the most competitive candidate with nickel-based superalloys in the automotive and aerospace industries because of their excellent mechanical properties in the temperature range from 600 to 1000 °C [1–9]. However, the as-cast TiAl alloys show a microstructure with coarse dendrites and composition segregation, leading to premature failures such as high fatigue crack growth rate, low fracture toughness, and poor ductility [10–13].

To achieve a strength and ductility balance of TiAl alloy, methods are employed to refine the grain size, such as the addition of interstitial elements such as boron [14–16], nitrogen [17], phase transformation via heat treatment [11,18,19], laser beam oscillation [20], and ultrasonic vibration [21]. It is found that 1.0 at.% nitrogen addition leads to remarkable grain refinement in the lamellar microstructure with an increase in yield strength by two times at room temperature. As α is the first precipitated phase in the reported alloy (Ti-48.5Al-1.5Mo), the TiN or Ti_2AlN precipitate acts as the nucleation site during the formation of the α phase [17]. Nitrogen ion was implanted into a β-solidifying γ-TiAl alloy. As Ti is a strong nitride former, several kinds of compounds were found, such as TiN, Ti_2N, Ti_3AlN, and $Ti_3Al_2N_2$, according to the nitrogen volume content and chemical composition [22]. With the addition of 2.5 at.% N into high Nb containing Ti-46Al-8Nb TiAl alloy, interstitial nitrogen atoms are proved to expand and stabilize the α phase region. Meanwhile, the average colony size of α phase decreases to around 5% of the size without nitrogen addition. The mechanism of α colony refinement is proposed as the diffusion of solute Al is suppressed by nitrogen at the solid–liquid interface, leading to α as the primary phase solidifies ahead of β [23].

Grain refinement by massive γ transformation requires heat treatment followed by oil/water quenching. It results in cracks and makes it difficult for manufacturing [19].

Another way of grain refinement is nucleation on borides in TiAl phase transformation. The addition of 1 wt.% boron in the alloy forms several kinds of borides, such as titanium monoboride (TiB), diboride (TiB_2), or Ti_3B_4 as nucleation sites at the beginning of solidification. Because borides cause strong constitutional undercooling in the segregation zone, it leads to lots of nucleation sites in the interdendritic area [14]. They create an opportunity for α to nucleate heterogeneously on borides during $\beta \rightarrow \alpha$ transformation, besides nucleation on β grain boundary. However, the cooling rate plays an important role in the nucleation of borides. Oehring [24] and Liu [4,10,25] have reported that heterogeneous nucleation of α grains on borides are strongly suppressed when the temperature gradient is high, especially when samples are laser beam welded or water quenched from high to room temperature.

The α grains prefer to nucleate on the β grain boundary with Burgers orientation relationship $\{110\}_\beta // (0001)_\alpha$ and $< 111 >_\beta // < 11\bar{2}0 >_\alpha$ during $\beta \rightarrow \alpha$ transformation [1]. It is found that although α grains are of fine plate morphology, these α grains originate from the same parent β, i.e., they are in the form of textured colonies [26]. Thus, due to two factors: (1) the effect of boride for α grain refinement is strongly suppressed at a high-temperature gradient; (2) the size of α colonies is predetermined by their parent β, it is extremely important to pay attention to refine primary β grains.

It thus comes to the idea to employ nuclei which precipitate as the first solid phase from melt for β grain refinement. According to the Ti-N phase diagram, the solidification temperature of TiN is found to be in the range from 2930 °C to 3290 °C [22,27], which is significantly higher than that of β (1670 °C) [1] and brings the possibility to employ TiN as a nucleant for β grain refinement. The present work brings a novel approach that grain refinement would work despite of high cooling rate. The size of α_2 textured colonies would be reduced even though it undergoes fast cooling. It sheds light on a method for mechanical property improvement.

2. Material and Methods

The examined alloy has the chemical composition Ti-42Al-2.5Cr-1Nb-0.7Si-0.5B (at. %). The actual composition is verified by energy dispersive spectroscopy (EDS) to within 1% of the nominal value. The substrate was cast, hot isostatic pressed, and cut by electro-discharge machining into small pieces with a geometry of 30 × 30 × 2.5 mm. The panels were then cleaned and sanded with 800# and 2000# SiC paper to remove oxides and machining debris. The welding process was performed using a 10 kW IPG Ytterbium fiber laser, as shown in Figure 1. The movement of the welding head in the x-y-z coordinate system is controlled by a KUKA KR30 HA robot (Shanghai, China). The sample (Sample 1#) was butt welded under argon. For comparison, the other sample (Sample 2#) was welded with the same parameters under a mixed atmosphere with argon and nitrogen as shielding gas, with each gas taking up 50% in volume. Before and after welding, laser scans back and forth along the welding seam 10 times for preheating and post-weld heat treatment.

After welding, a visual inspection was carried out on the weld. The welded samples were cut, ground, and polished, and followed by mechanical polishing with a vibratory polisher. The microstructure was analyzed using scanning electron microscopy (SEM, Zeiss, Germany) in backscattered electron (BSE) mode, energy dispersive spectroscopy (EDS), and electron backscattered diffraction (EBSD). The phases were analyzed by micro-X-ray diffraction (mXRD) using CuKα radiation to examine the phase composition and microstructure of the nitride in alloys. The measurement size is 0.5 × 0.5 μm. After the experiment, the recorded Debye–Scheller diffraction rings are azimuthally integrated to obtain the diffraction pattern as a function of the scattering vector q: $q = 4\pi \sin(\theta)/\lambda$, where θ is the diffraction angle and λ is the wavelength of the X-ray beam.

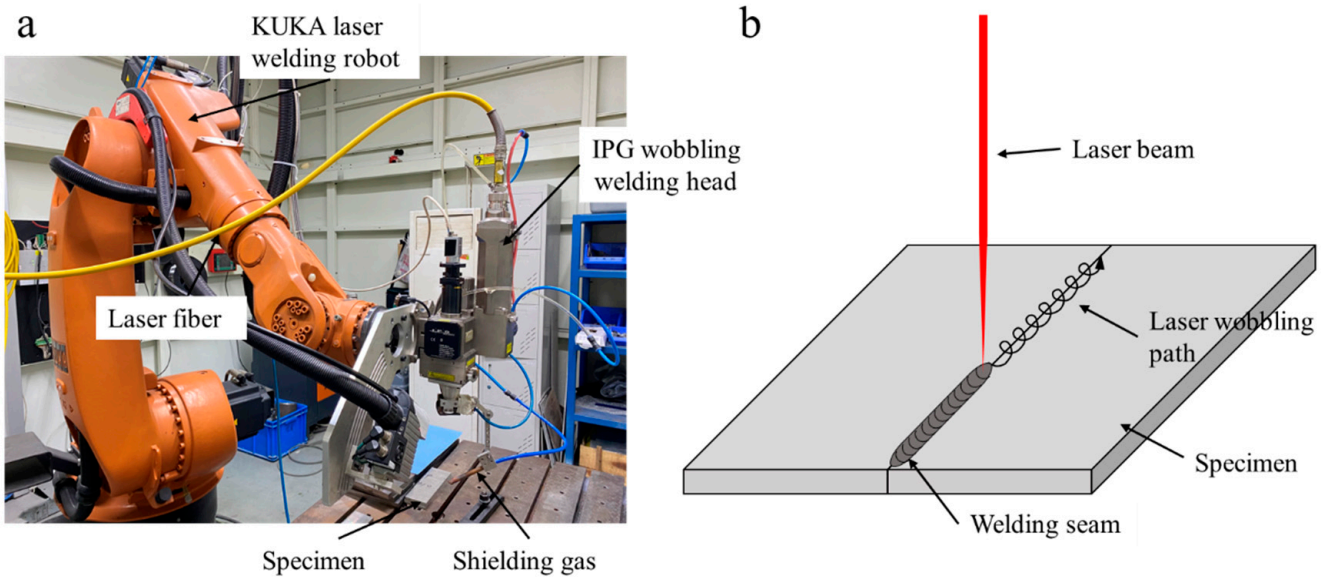

Figure 1. The robot-controlled laser beam welding system with a beam scanning function. (**a**) Actual experimental setup. (**b**) Schematic diagram of the experimental setup.

3. Results and Discussion

Figure 2a shows the microstructure of the substrate. In the backscattered electron mode, γ-TiAl is dark, α_2 + γ lamellae is light gray, and B2 is the brightest phase. EDS analysis of Ti-32.78Al-2.6Cr-1.2Nb-1.05Si proves that the B2 phase is rich in Nb and Ti and deficient in Al. The Ti-Al phase diagram [1] shows the melt with the composition of Ti-42Al undergoes the following phase transformations from high to room temperature: Liquid → Liquid + β → β →α + β→α + γ+ β→α_2 + γ + B2. The arrows indicated phase, with dotted morphology and bright color, are observed in the lamellar colony interior. They are indicated as borides, with the composition of TiB, TiB_2, and Ti_3B_4, depending on their chemical composition [26,28,29]. These borides have been reported to be essential in grain refinement through the heterogeneous nucleation of α on borides [30,31].

The weld zone of the 1# sample (Figure 2b) consists of fine needle-like α_2 plates distributed in any direction. Figure 2c shows details of the microstructure, and the average width of α_2 plates is 1.12 μm. There are bright ridges located between the fine acicular α_2 plates. As analyzed by EDS, bright ridges are enriched in Cr and Nb by ejecting heavy elements into the inter-lamellar region during the β→α transition [15,32].

The welding zone of sample 2# (Figure 2d) is composed of dendrites. These dendrites are randomly orientated in the welding zone with an average length of 28 μm. Some dendrites are in the form of lots of dots because the dendrites were cut through by the exam surface. As shown in Figure 2e, the core of the dendrite is a bright color and is surrounded by dark islands. Some bright interlayers are located between the dark islands.

As shown in Figure 3a, a linear EDS scan was carried out to verify the chemical composition of dendrites. The dendritic arm is enriched with Ti and N, with around 70 at.% of Ti and 30 at.% of N. Meanwhile, Al is depleted from the dendrite with a content less than 10 at.%. For phase identification, XRD analysis was carried out. It shows in the welding zone of sample 1#, α_2 and γ phases are identified. In contrast, the welding zone of sample 2# consists of TiN, α_2, and γ (Figure 3b). Combining EDS and XRD analysis, the dendrites are defined as TiN.

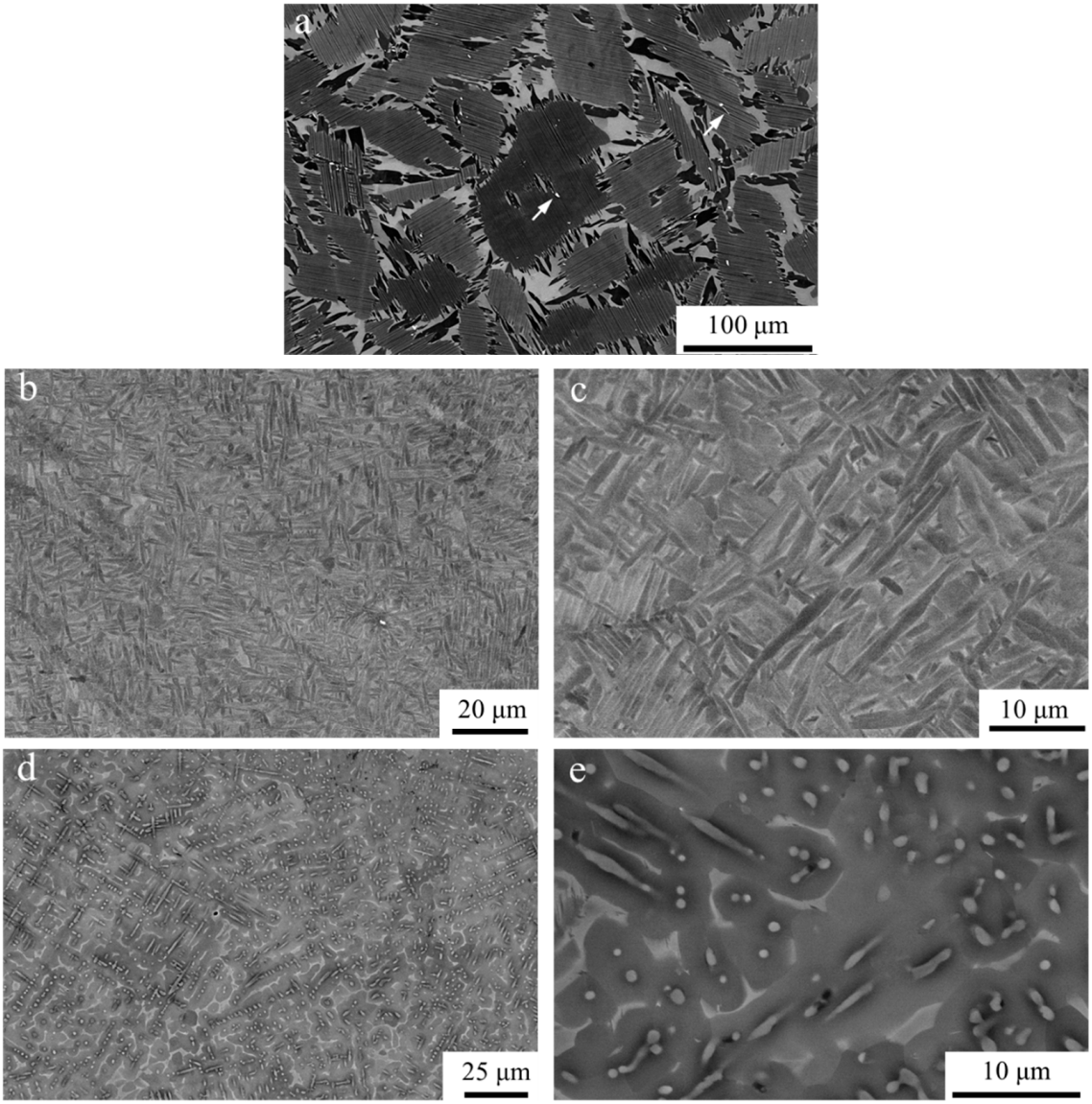

Figure 2. Microstructure of (**a**) base metal, (**b**,**c**) weld zone of sample 1#, (**d**,**e**) detailed microstructure of weld of sample 2# in backscattered electron (BSE) mode SEM image taken from the area and detailed microstructure.

From the microstructure (Figure 2b) and EBSD (Figure 4a) observation, the α_2 plates in the weld zone are distributed by chance. However, with careful inspection, it is found that lots of α_2 plates are orientated in the same direction, as they are colored the same. These α_2 plates can even be separated into groups. There is a group of α_2 plates located over 80% of the measured area (Figure 4a). As indicated in Figure 4c,f, the basal plane orientations of these α_2 plates are presented, showing they are with misorientation angles of 60° or 90° between the plates. These positions of the (0001) α_2 poles correspond well with $(111)_\beta$ plane of one β grain. B → α transformation follows Burgers orientation relationship $\{0001\}_\alpha // \{110\}_\beta$ and $< 11\bar{2}0 >_\alpha // < 111 >_\beta$. According to Gey and Humbert, misorientation angles of Burgers α variants originating from the same parent β grain can only obey angles of 0°, 10.5°, 60°, 60.8° and 90°, including parallel orientations [33]. On the other hand, when neighboring α grains obey such misorientation angles, they can be determined as α grains from the same parent β. Due to this effect, the size of the colony in the welding zone cannot be easily identified from the size of the α_2 plate. The size of the "textured colonies" should be counted.

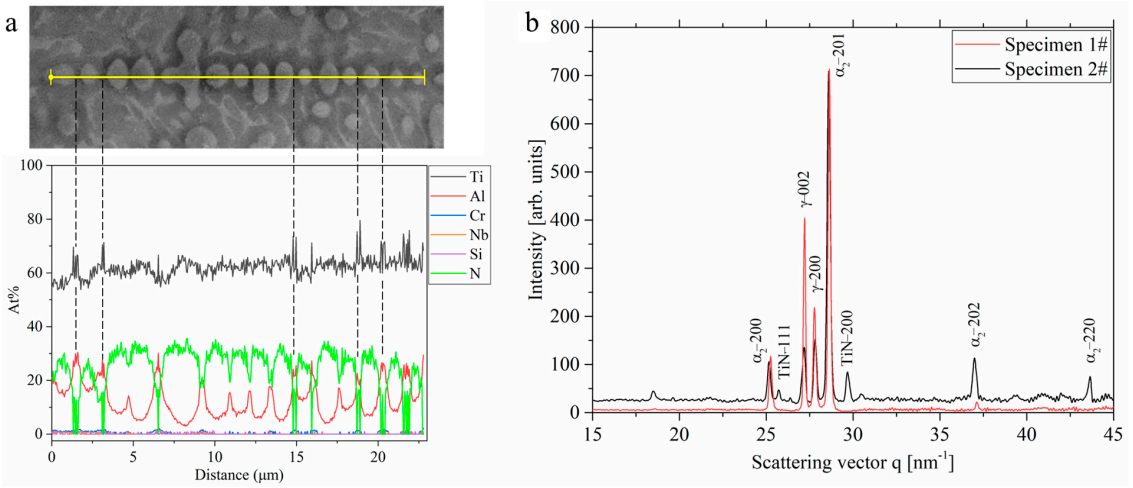

Figure 3. (**a**) Chemical composition analysis of dendrite by EDS and (**b**) micro-area XRD of welding zone in samples 1# and 2#.

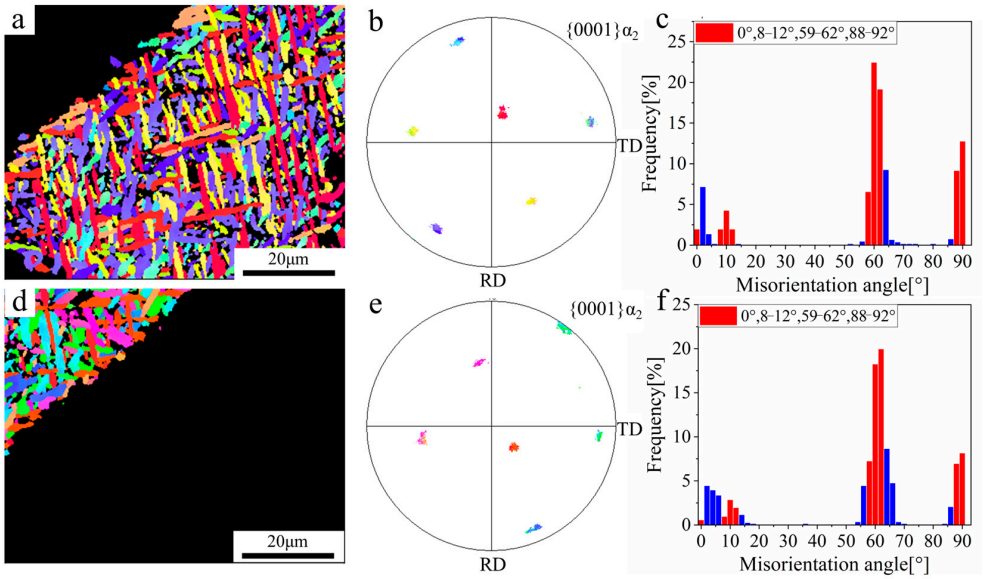

Figure 4. EBSD measurement of α_2 phase in the weld zone of sample 1#. Two groups are divided. (**a**,**d**) are texture maps of each group; (**b**,**e**) are pole figures of each group; (**c**,**f**) are corresponding misorientation angles.

Figure 5a is the α_2 phase texture map. All the α_2 grains are orientated in different directions. The dendrites, which are presented in black color, are located in the middle of α_2 grains. In the $\{0001\}\alpha_2$ pole figure, basal planes of the α_2 phase are randomly distributed. The misorientation angles between neighboring α_2 grains are shown in Figure 5c. There is a limited preference for 0–2°, 8–12°, 58–62°, and 88–92°, which indicates that the α_2 grains are not stemmed from the same parent β. However, after careful examination, it was found that these α_2 grains are in six groups, as illustrated in Figure 5d,g,j,m,p,s. In each group, the basal planes of these α_2 grains are in a relationship with their neighboring TiN grains $\{111\}_{TiN}//\{0001\}_{\alpha_2}$, as shown in Figure 5e,f,h,i,k,l,n,o,q,r,t,u. Because α grains follow the Burgers orientation relationship with β $\{110\}_\beta//(0001)_\alpha$, it can be inferred that the primary β grain is in an orientation relationship with TiN $\{111\}_{TiN}//\{110\}_\beta$. The size of the α_2 grain group corresponds to the size of their primary β. According to the particle interval counting method proposed by ASTM E112-10 [34], the average diameter of the colonies (considered as β particles) is 35 μm. The colony size is similar to the dendrite length of TiN.

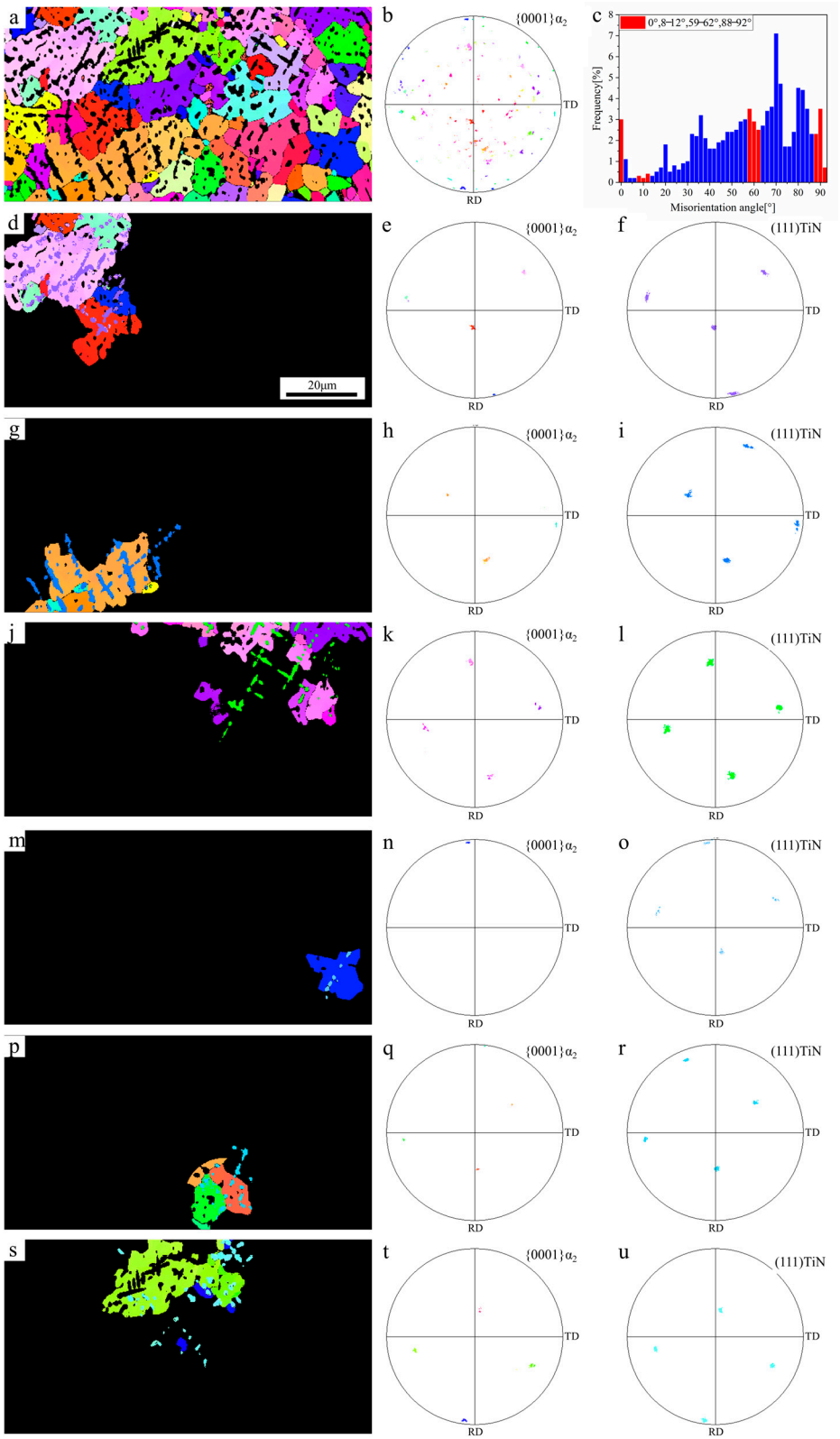

Figure 5. EBSD measurements of TiN and α_2 phase of the welding zone of 2# sample: (**a**) α_2 texture map; (**b**) α_2 phase pole figure; (**c**) corresponding misorientation angles of α_2 phase; (**d**,**g**,**j**,**m**,**p**,**s**) texture map of TiN and α_2 phase of sections 1–6, (**e**,**h**,**k**,**n**,**q**,**t**) pole figure of (0001) α_2 in each section; (**f**,**i**,**l**,**o**,**r**,**u**) pole figure of (111) TiN in each section.

The formation of TiN is proposed as a three-step mechanism, i.e., deposition, diffusion, and reaction. In the first step, nitrogen decomposes during interaction with the laser into atomic nitrogen, which is a more effective nitrifier than molecular nitrogen. During welding, TiAl is first melted by a laser beam and driven by convection, resulting in exposure of the melt to nitrogen atoms [35]. When an excessive amount of nitrogen has dissolved in the liquid up to its solubility limit, there is an exothermic reaction with the liquid that leads to the formation of TiN:

$$\mathrm{Ti}+\frac{1}{2}\mathrm{N_2}=\mathrm{TiN}$$

As Ti and N present stronger chemical affinity than that of Al and N [36], atomic nitrogen absorps into the melting pool, diffuses into the melt, and reacts with Ti atoms to form Ti–N binary compounds. Several kinds of compounds could form, such as TiN, Ti_2N, and Ti_3AlN, according to the nitrogen volume content and chemical composition of the alloy. In the present work, only TiN is found. As Ti atoms diffuse towards the nitrogen-rich locations to form TiN, the Al are depleted between the nitride dendrites.

As the solidification temperature of TiN is higher than that of β. It can be inferred that TiN first precipitates from the melt. With the aid of a nitrogen atmosphere, the solidification path is modified into L → TiN + L → TiN + β → TiN + α + γ → TiN + α_2 + γ. As the temperature goes down, the β grains start to nucleate. In sample 1#, β grains homogeneously nucleate due to undercooling. Compared with sample 2#, a large amount of suspending TiN serves as heterogeneous nucleation sites for β. It can be inferred that the intake of nitrogen into the melting pool significantly increases the nucleation sites for β due to the fact that there is a large amount of TiN swimming in the melt, which is evidenced by Figure 6. An excessive amount of β nuclei brings a higher possibility for β to interact with each other as they grow, leading to β grain refinement. Thus, the nucleated β grains are significantly refined when nitrogen is applied as shielding gas.

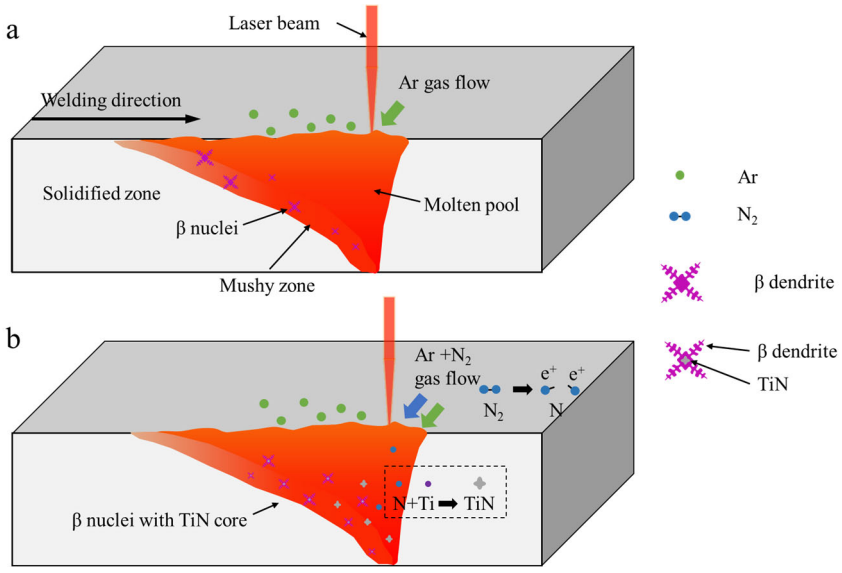

Figure 6. Schematic presentation of the nucleation condition in (**a**) sample 1# and (**b**) sample 2#.

4. Conclusions

Refined α_2 textured colonies are obtained during laser beam welding with nitrogen as shielding gas. This study shed light on a novel approach to microstructure refinement of TiAl despite of high cooling rate, such as laser welding.

(1) When argon is employed as a shielding gas, a large amount of α_2 textured colonies is formed at a high cooling rate due to the formation of coarse β grain. Nitrogen decomposes into atomic nitrogen, diffuses into the melt, reacts with Ti, and finally forms a TiN compound.

(2) The suspending TiN swimming in the melt serves as heterogeneous nucleation sites for β. The β grains are found to nucleate heterogeneously on the TiN with an orientation relationship $\{111\}_{TiN}//\{110\}_{\beta}$. An excessive amount of β nuclei brings a higher possibility for β to interact with each other as they grow, leading to refined β grains.
(3) The orientation relationship of α_2 grains with their neighboring TiN grains is determined as $\{111\}_{TiN}//\{0001\}_{\alpha_2}$.
(4) Due to the excellent refinement function of TiN, in the next step, a certain amount of TiN particles could be considered to add into the melt for grain refinement.

Author Contributions: Conceptualization, J.L. and S.G.; methodology, L.W.; software, T.W.; writing—original draft preparation, J.L.; writing—review and editing, J.L.; supervision, P.Z., T.M. and Z.W.; project administration, K.W. All authors have read and agreed to the published version of the manuscript.

Funding: This research was financially supported by Natural Science Foundation of Jiangsu Province (No. BK20200502); Natural Science Foundation of Hunan Province (No. 2021JJ40761) and China Postdoctoral Science Foundation (No. 2021M691588).

Data Availability Statement: Not applicable.

Conflicts of Interest: The authors declare no conflict of interest.

References

1. Appel, F.; Paul, J.D.H.; Oehring, M. *Gamma Titanium Aluminide Alloys Science and Technology*; WILEY-VCH: Weinheim, Germany, 2011.
2. Clemens, H.; Mayer, S. Design, Processing, Microstructure, Properties, and Applications of Advanced Intermetallic TiAl Alloys. *Adv. Eng. Mater.* **2013**, *15*, 191–215. [CrossRef]
3. Kong, F.T.; Cui, N.; Chen, Y.Y.; Wang, X.P. A Novel Composition Design Method for Beta-Gamma TiAl Alloys with Excellent Hot Workability. *Metall. Mater. Trans. A* **2018**, *49A*, 5574–5584. [CrossRef]
4. Liu, J.; Staron, P.; Riekehr, S.; Stark, A.; Schell, N.; Huber, N.; Schreyer, A.; Mueller, M.; Kashaev, N. Phase Transformations During Solidification of a Laser-Beam-Welded TiAl Alloy-An In Situ Synchrotron Study. *Metall. Mater. Trans. A—Phys. Metall. Mater. Sci.* **2016**, *47A*, 5761–5770. [CrossRef]
5. Song, L.; Wang, L.; Oehring, M.; Hu, X.; Appel, F.; Lorenz, U.; Pyczak, F.; Zhang, T. Evidence for deformation twinning of the D0(19)-alpha(2) phase in a high Nb containing TiAl alloy. *Intermetallics* **2019**, *109*, 91–96. [CrossRef]
6. Xu, X.; Hu, R.; Lin, J.; Guo, J. Evolution of Microstructure and Microsegregation of Ti-45Al-8Nb Alloy during Directional Solidification. *Adv. Mater. Sci. Eng.* **2018**, *2018*, 1713835. [CrossRef]
7. Salvador, C.A.F.; Maia, E.L.; Costa, F.H.; Escobar, J.D.; Oliveira, J.P. A compilation of experimental data on the mechanical properties and microstructural features of Ti-alloys. *Sci. Data* **2022**, *9*, 188. [CrossRef]
8. Callegari, B.; Oliveira, J.P.; Aristizabal, K.; Coelho, R.S.; Brito, P.P.; Wu, L.; Schell, N.; Soldera, F.A.; Mücklich, F.; Pinto, H.C. In-situ synchrotron radiation study of the aging response of Ti-6Al-4V alloy with different starting microstructures. *Mater. Charact.* **2020**, *165*, 110400. [CrossRef]
9. Callegari, B.; Oliveira, J.P.; Coelho, R.S.; Brito, P.P.; Schell, N.; Soldera, F.A.; Mücklich, F.; Sadik, M.I.; García, J.L.; Pinto, H.C. New insights into the microstructural evolution of Ti-5Al-5Mo-5V-3Cr alloy during hot working. *Mater. Charact.* **2020**, *162*, 110180. [CrossRef]
10. Liu, J.; Dahmen, M.; Ventzke, V.; Kashaev, N.; Poprawe, R. The effect of heat treatment on crack control and grain refinement in laser beam welded beta-solidifying TiAl-based alloy. *Intermetallics* **2013**, *40*, 65–70. [CrossRef]
11. Chen, L.; Lin, J.; Xu, X.; Li, C.; Xu, Y.; Liang, Y. Microstructure refinement via martensitic transformation in TiAl alloys. *J. Alloys Compd.* **2018**, *741*, 1175–1182. [CrossRef]
12. Wang, X.; Xu, W.; Xu, P.; Zhou, H.; Kong, F.; Chen, Y. High Nb–TiAl Intermetallic Blades Fabricated by Isothermal Die Forging Process at Low Temperature. *Metals* **2020**, *10*, 757. [CrossRef]
13. Oliveira, J.P.; Shamsolhodaei, A.; Shen, J.; Lopes, J.G.; Gonçalves, R.M.; de Brito Ferraz, M.; Piçarra, L.; Zeng, Z.; Schell, N.; Zhou, N.; et al. Improving the ductility in laser welded joints of CoCrFeMnNi high entropy alloy to 316 stainless steel. *Mater. Des.* **2022**, *219*, 110717. [CrossRef]
14. Cheng, T.T. The mechanism of grain refinement in TiAl alloys by boron addition—An alternative hypothesis. *Intermetallics* **2000**, *8*, 29–37. [CrossRef]
15. Hu, D. Effect of boron addition on tensile ductility in lamellar TiAl alloys. *Intermetallics* **2002**, *10*, 851–858. [CrossRef]
16. Gosslar, D.; Günther, R.; Hecht, U.; Hartig, C.; Bormann, R. Grain refinement of TiAl-based alloys: The role of TiB2 crystallography and growth. *Acta Mater.* **2010**, *58*, 6744–6751. [CrossRef]
17. Yun, J.H.; Wee, D.M.; Oh, M.H.; Inui, H.; Yamaguchi, M. Nitrogen-doped TiAl alloys Part I Microstructure control. *J. Mater. Sci.* **2000**, *35*, 4527–4532. [CrossRef]

18. Clemens, H.; Bartels, A.; Bystrzanowski, S.; Chladil, H.; Leitner, H.; Dehm, G.; Gerling, R.; Schimansky, F.P. Grain refinement in γ-TiAl-based alloys by solid state phase transformations. *Intermetallics* **2006**, *14*, 1380–1385. [CrossRef]
19. Wu, X.; Hu, D. Microstructural refinement in cast TiAl alloys by solid state transformations. *Scr. Mater.* **2005**, *52*, 731–734. [CrossRef]
20. Liu, J.; Wang, M.; Zhang, P.; Chen, Y.; Wang, S.; Wu, T.; Xie, M.; Wang, L.; Wang, K. Texture refinement and mechanical improvement in beam oscillation superimposed laser welding of TiAl-based alloy. *Mater. Charact.* **2022**, *188*, 111892. [CrossRef]
21. Ruirun, C.; Deshuang, Z.; Jingjie, G.; Tengfei, M.; Hongsheng, D.; Yanqing, S.; Hengzhi, F. A novel method for grain refinement and microstructure modification in TiAl alloy by ultrasonic vibration. *Mater. Sci. Eng. A* **2016**, *653*, 23–26. [CrossRef]
22. Panov, D.O.; Sokolovsky, V.S.; Stepanov, N.D.; Zherebtsov, S.V.; Panin, P.V.; Nochovnaya, N.A.; Salishchev, G.A. Oxidation resistance and thermal stability of a β-solidified γ-TiAl based alloy after nitrogen ion implantation. *Corros Sci.* **2020**, *177*, 109003. [CrossRef]
23. Zhang, T.; Wu, Z.; Hu, R.; Zhang, F.; Kou, H.; Li, J. Influence of nitrogen on the microstructure and solidification behavior of high Nb containing TiAl alloys. *Mater. Des.* **2016**, *103*, 100–105. [CrossRef]
24. Oehring, M.; Stark, A.; Paul, J.D.H.; Lippmann, T.; Pyczak, F. Microstructural refinement of boron-containing beta-solidifying gamma-titanium aluminide alloys through heat treatments in the beta phase field. *Intermetallics* **2013**, *32*, 12–20. [CrossRef]
25. Liu, J.; Staron, P.; Riekehr, S.; Stark, A.; Schell, N.; Huber, N.; Schreyer, A.; Mueller, M.; Kashaev, N. Phase Transformation and Residual Stress in a Laser Beam Spot-Welded TiAl-Based Alloy. *Metall. Mater. Trans. A—Phys. Metall. Mater. Sci.* **2016**, *47A*, 5750–5760. [CrossRef]
26. Liu, J.; Wu, T.; Wang, M.; Wang, L.; Zhou, Q.; Wang, K.; Staron, P.; Schell, N.; Huber, N.; Kashaev, N. In situ observation of competitive growth of α grains during β → α transformation in laser beam manufactured TiAl alloys. *Mater. Charact.* **2021**, *179*, 111371. [CrossRef]
27. Wriedt, H.A.; Murray, J.L. The N-Ti (Nitrogen-Titanium) system. *Bull. Alloy. Phase Diagr.* **1987**, *8*, 378–388. [CrossRef]
28. Han, J.; Xiao, S.; Tian, J.; Chen, Y.; Xu, L.; Wang, X.; Jia, Y.; Du, Z.; Cao, S. Grain refinement by trace TiB2 addition in conventional cast TiAl-based alloy. *Mater. Charact.* **2015**, *106*, 112–122. [CrossRef]
29. Hecht, U.; Witusiewicz, V.; Drevermann, A.; Zollinger, J. Grain refinement by low boron additions in niobium-rich TiAl-based alloys. *Intermetallics* **2008**, *16*, 969–978. [CrossRef]
30. Clemens, H.; Kestler, H. Processing and Applications of Intermetallic γ-TiAl-Based Alloys. *Adv. Eng. Mater.* **2000**, *2*, 551–570. [CrossRef]
31. Hu, D. Role of boron in TiAl alloy development: A review. *Rare Met.* **2016**, *35*, 1–14. [CrossRef]
32. Hu, D.; Huang, A.J.; Novovic, D.; Wu, X. The effect of boron and alpha grain size on the massive transformation in Ti-46Al-8Nb-xB alloys. *Intermetallics* **2006**, *14*, 818–825. [CrossRef]
33. Gey, N.; Humbert, M. Characterization of the variant selection occurring during the alpha ->beta ->alpha phase transformations of a cold rolled titanium sheet. *Acta Mater.* **2002**, *50*, 277–287. [CrossRef]
34. *ASTM E112-13*; Standard Test Methods for Determining Average Grain Size. ASTM: Montgomery County, PA, USA, 2010.
35. Nwobu, A.I.P.; Rawlings, R.D.; West, D.R.F. Nitride formation in titanium based substrates during laser surface melting in nitrogen–argon atmospheres. *Acta Mater.* **1999**, *47*, 631–643. [CrossRef]
36. Zhao, B.; Sun, J.; Sheng Wu, J.; Xin Yuan, Z. Gas nitriding behavior of TiAl based alloys in an ammonia atmosphere. *Scr. Mater.* **2002**, *46*, 581–586. [CrossRef]